RFID Tag Localization with a Sparse Tag Array

Chao Yang, Xuyu Wang, and Shiwen Mao, *Fellow, IEEE*

Abstract—With the rapid growth of the Internet of Things (IOT), the Radio Frequency Identification (RFID) technology has been recognized as an effective and low-cost solution for many IoT applications. In this paper, we study the problem of utilizing a sparse RFID tag array for backscatter indoor localization. We first theoretically and experimentally validate the feasibility of using sparse tag arrays for direction of arrival (DOA) estimation. We then present the SparseTag system, which leverages a novel sparse tag array for high-precision backscatter indoor localization. The SparseTag system includes sparse array processing, difference co-array design, DOA estimation using a spatial smoothing based method, and a localization method. A robust channel selection method based on the RFID tag array is adopted for mitigating the multipath effect. The SparseTag system is implemented with commodity RFID devices. Its superior performance is validated in two different environments with extensive experiments and comparison to baseline schemes.

Index Terms—Radio Frequency Identification (RFID), indoor localization, direction of arrival (DOA), sparse array, difference co-array.

1 Introduction

With the rapid growth of the Internet of Things (IOT), the Radio Frequency Identification (RFID) technology has been regarded as an effective and low-cost solution for many emerging IoT applications. In addition to the wide adoption in traditional identification applications in various fields, such as retailing, sports, library, manufacturing, and supply chain management, positioning of RFID tags has attracted increasing interest from researchers in recent years. Rather than reading the stored Electronic Product Code (EPC) from RFID tags, the low level data of the RFID channel, such as received signal strength indication (RSSI) and phase, can be collected from the received tag responses and leveraged for tag localization.

RSSI-based technique has been proposed to localize RFID tags [2], but the accuracy of such systems is usually limited by the low resolution and randomness of the RSSI data. Active RFID tags have been adopted in prior works, which usually has a much higher cost than the passive tags. For passive tag based localization, phase angle has been widely utilized because of its high resolution and stability. However, due to the wide beam of polarized reader antenna and the multipath effect, high-accuracy positioning of passive tags is still a big challenge. To achieve narrow beams of the reader antenna for high-accuracy localization, multiple antennas can be utilized [3], [4], but at a higher cost. Systems with a single moving antenna or moving RFID tags are then proposed for reduced cost [5]–[7], which generate additional virtual antennas instead of using real ones. These techniques can achieve high localization accuracy, but the moving the antenna or tag incurs time delay and requires careful calibration of the system.

Recently, RFID tag array has been leveraged to improve the accuracy and the robustness of RFID-based sensing systems [1], [8]. For example, Tagyro uses a hologram-based method to transform phase offset to orientation of the tag array [9] for tracking the 3D orientation of passive objects. RF-Wear is developed for orientation estimation with a uniform linear array (ULA) for body-frame tracking [10]. The accuracy of direction of arrival (DOA) based localization techniques can be improved by utilizing more antennas. Thus leveraging a tag array with more RFID tags is an effective way to achieve high positioning accuracy. Compared with the systems with multiple polarized antennas, the cost of building a passive RFID tag array is negligible.

However, the technical challenges still exist for tag array-based localization, such as how to mitigate the multipath effect from the propagation environments and the phase distortion caused by mutual coupling between RFID tags. To deal with the influence of multipath effect, some existing techniques leverage a mobile antenna to localize a tag array in different positions [11], [12]. Although the mobile antenna can reduce the cost, the specialized mobile shelf and motor incur additional cost. For DOA based localization, the multipath effect could be effectively mitigated by utilizing an RFID tag array with sufficient number of tags.

However, when the traditional ULA tag array is used, the tag density could be high when many tags are placed on a small surface of the object, such as a book or a small package. In such scenarios, the accuracy will be influenced by the strong mutual coupling effect, which introduces additional frequency offset as well as amplitude offset of the resonance peak [13], [14]. It has been proved by several existing systems that mutual coupling generates considerable interference to the collected phase angle of RFID tags, which degrades the localization performance [15], [16]. Furthermore, the backscattered signal from RFID tags may not be sufficiently strong to be detected by the antenna, because the strength of the signal is also affected by mutual coupling. Thus, a special tag array with a lower density

- *C. Yang and S. Mao are with the Department of Electrical and Computer Engineering, Auburn University, Auburn, AL 36849-5201, USA. X. Wang is with the Department of Computer Science, California State University, Sacramento, CA 95819-6021, USA.*
  Email: czy0017@auburn.edu, xuyu.wang@csus.edu, smao@ieee.org.
- *This work is supported in part by the NSF under Grants ECCS-1923163 and CNS-2105416, and through the Wireless Engineering Research and Education Center (WEREC) at Auburn University. This work was presented in part at The 2019 IEEE International Conference on Sensing, Communication and Networking, June 2019, Boston, MA.*
- *DOI: 10.1109/JIOT.2021.3137723.*

than ULA is needed, to be resilient to mutual coupling and deliver accurate DOA estimation.

In this paper, we propose a novel sparse RFID tag array for tag localization [1]. We first an analysis of the mutual coupling effect and prove that the phase difference from pairs of tags used in our system is independent to the coupled voltage and mutual impedance. Next, we present the SparseTag system, i.e., a **Sparse** RFID **Tag** array system for high-precision backscatter indoor localization, which comprise a sparse tag array and an RFID reader with two antennas. We analyze our sparse array processing for DOA estimation, which is quite different from the traditional MUSIC algorithm based methods using a ULA [17]. The key idea is to obtain a new signal vector with a difference co-array, which is a longer array whose antenna locations are not evenly spaced. In addition, we design a new sparse RFID tag array, which has a symmetric structure and is effective for mitigating the mutual coupling effect. We derive its difference co-array and prove its several important properties, such as its hole-free feature, degrees of freedom (DOF), and weight function. We analytically show why the proposed sparse tag array can outperform ULA on DOA estimation. Then, we develop a DOA estimation scheme using the difference co-array of the proposed sparse tag array with a spatial smoothing method. Finally, we provide a localization method based on the two estimated DOAs, while a robust channel selection method is proposed for mitigating the multipath effect. We implement SparseTag with off-the-shelf RFID tags and reader, and evaluate its performance in two environments, including a computer laboratory and an anechoic chamber, where superior DOA estimation and location performance over the ULA-based benchmark scheme are demonstrated.

The main contributions made in this paper are summarized as follows.

- We justify the feasibility and advantages of utilizing a sparse tag array for DOA based indoor localization through analysis and experiments. To the best of our knowledge, this is the first work to leverage sparse tag arrays for backscatter indoor localization, which does not require to move either the tags or the antenna(s).
- We design the SparseTag system, which includes sparse array processing, difference co-array design, DOA estimation using a spatial smoothing based method, and a localization method. We propose a new sparse tag array design and analytically prove its superior performance over the traditional ULA design. In addition, a robust channel selection method based on the sparse tag array is proposed for mitigating the indoor multipath effect.
- We implement SparseTag with off-the-shelf RFID tags and reader, and evaluate its performance in two indoor environments, including a computer laboratory and an anechoic chamber, with extensive experiments. The experimental results verify the effectiveness of the proposed SparseTag system.

The remainder of this paper is organized as follows. We analyze the mutual coupling effect on RFID phase difference and the success rate of sampling in Section 2. The proposed SparseTag system is presented in Section 3 and its performance is evaluated in Section 4. Section 5 discusses related work and Section 6 concludes this paper.

2 Analysis of Mutual Coupling

2.1 Phase Angle and Phase Difference

The FCC requires frequency hopping to avoid interference for readers. The readers use the spectrum between 902.5 MHz and 927.5 MHz, which is divided into 50 channels. The reader uses the Low-Level Reader Protocol (LLRP) to interrogate tags, which can provide RF phase angle, Doppler frequency, and Peak RSSI of the channel [18]. In particular, the phase angle, denoted by ϕ, can be written as

$$\phi = \mathrm{mod}\left(\frac{2\pi \cdot 2l}{\lambda} + \theta_t + \theta_r + \theta_{tag}, 2\pi\right), \quad (1)$$

where l is the distance between the tag and the reader antenna, λ is the wavelength of the signal, and θ_t, θ_r, and θ_{tag} are the offsets introduced by the reader's transmitting circuit, the reader's receiving circuit, and the RFID tag's backscattering circuit, respectively. The challenge for RFID-based sensing techniques is how to translate the measured phase ϕ to distance l, under strong interference from the phase offsets and frequency hopping.

To mitigate the impact of phase offsets, we propose to adopt an RFID tag array. Rather than using the phase angle from each individual tag, the difference between a pair of neighboring tags is used. Following (1), the phase difference between Tags 1 and 2 is given by

$$\Delta\phi_{1,2} = \mathrm{mod}\left(\frac{2\pi \cdot 2(l_1 - l_2)}{\lambda} + \theta_{tag_1} - \theta_{tag_2}, 2\pi\right), \quad (2)$$

where l_1 and l_2 are the distances from Tags 1 and 2 to the reader antenna, respectively; and θ_{tag_1} and θ_{tag_2} are the phase offsets due to Tags 1 and 2's circuit, respectively. It can be seen that the phase offsets introduced by the reader's circuits, i.e., θ_t and θ_r, are canceled in (2). In addition, the incident wave from the reader antenna is similar to a plane wave if the tag-antenna distance is sufficiently long. In this case, the phase difference can be translated to the DOA, if the pair of tags are placed closer than $\lambda/4$ [16].

2.2 The Mutual Coupling Effect

When a tag array is deployed, the mutual coupling effect becomes a limiting factor of the sensing performance. The inductive coupling of neighboring RFID antennas causes transfer of energy between closely placed tags, which usually affect the measured phase angles and the received signal strength at the reader. In the remainder of this section, we will provide an analysis of the effects of mutual coupling on phase difference and sampling effectiveness.

2.2.1 Impact on Phase Angle and Phase Difference

The Gen 2 protocol is adopted for the interrogation process to avoid collision of simultaneous responses to a query from multiple tags [19]. With this protocol, among the tags that respond to the reader's query with their RN16 (a 16-bit random number), only one tag, to which the reader echoes

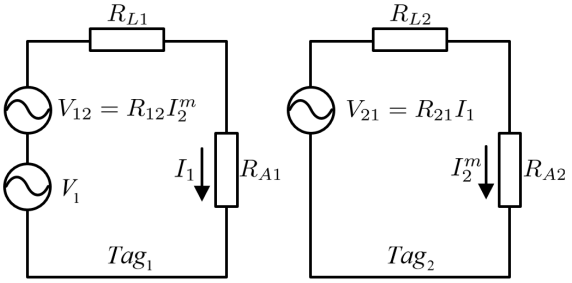

(a) When Tag 1 is activated.

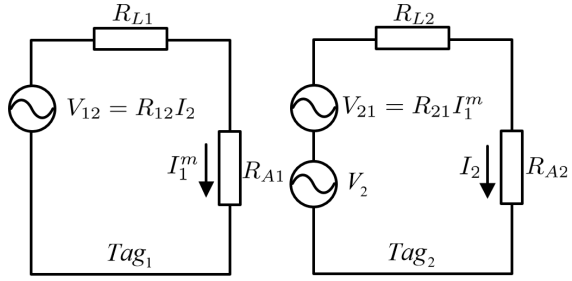

(b) When Tag 2 is activated.

Fig. 1. The equivalent circuit model of two tags under mutual coupling.

with its RN16, will be activated to send its EPC to the reader in every round of interrogation.

In Fig. 1, we present the corresponding circuit models of two tags under mutual coupling [20]. The upper plot is for the case when Tag 1 is activated, and the lower plot is for the case when Tag 2 is activated. In the circuit models, V_1 and V_2 represent the source voltages, and I_1 and I_2 are the source currents, when Tag 1 or Tag 2 is activated, respectively; R_{L1} and R_{L2} are the impedance of the microchip, and R_{A1} and R_{A2} are the impedance of the antenna input, of the two tags, respectively.

Theorem 1. *Consider two RFID tags under strong mutual coupling. If the tags have identical chip impedance and antenna input impedance, i.e., $R_{L1} = R_{L2}$ and $R_{A1} = R_{A2}$, the ratio of their equivalent source currents equals to the ratio of their equivalent source voltages. That is, we have $I_1/I_2 = V_1/V_2$.*

Proof. Consider the case when Tag 1 is activated by the reader. Due to induced coupling of the two tags' antennas, Tag 1's current I_1 will trigger a coupled voltage $V_{21} = R_{21} \cdot I_1$ in Tag 2. Here R_{21} is the mutual impedance of Tag 2 with respect to Tag 1. The coupled voltage V_{21} will then induce a current I_2^m in Tag 2, which next produces a coupled voltage $V_{12} = R_{12} \cdot I_2^m$ back at Tag 1, Here R_{12} is the mutual impedance in Tag 1 with respect to Tag 2. Assuming the two tags are of the same type, it follows that

$$I_1 \cdot (R_{L1} + R_{A1}) = I_1 \cdot R_0 = V_1 + R_{12} \cdot I_2^m \quad (3)$$
$$I_2^m \cdot (R_{L2} + R_{A2}) = I_2^m \cdot R_0 = R_{21} \cdot I_1, \quad (4)$$

where $R_0 = R_{L1} + R_{A1} = R_{L2} + R_{A2}$ is a constant. Assume the two tags have identical mutual impedance [20], i.e., $R_{12} = R_{21} = R_m$. Then current I_1 can be written as

$$I_1 = \frac{V_1}{R_0 - R_m^2/R_0}. \quad (5)$$

We can drive the same relationship for the case when Tag 2 is activated, as

$$I_1^m \cdot (R_{L1} + R_{A1}) = I_1^m \cdot R_0 = R_{12} \cdot I_2 \quad (6)$$
$$I_2 \cdot (R_{L2} + R_{A2}) = I_2 \cdot R_0 = V_2 + R_{21} \cdot I_1^m, \quad (7)$$

where I_1^m is the induced current in Tag 1 by the coupling voltage V_{12}. We can solve for the current I_2 in Tag 2 as

$$I_2 = \frac{V_2}{R_0 - R_m^2/R_0}, \quad (8)$$

Then we conclude from (5) and (8) that $I_1/I_2 = V_1/V_2$. □

Rewrite the complex current and voltages as $I_i = |I_i| \angle I_i$ and $V_i = |V_i| \angle V_i$, $i = 1, 2$, where $|\cdot|$ is the amplitude and $\angle$ is the phase angle. According to Theorem 1, we have

$$\angle I_1 - \angle I_2 = \angle V_1 - \angle V_2. \quad (9)$$

The measured phase angle by the reader is determined by the distance and the phase of the current that generates the tag response signal [21]. But the measured phase difference will be independent to the coupling voltage and mutual impedance. That is, *mutual coupling has a negligible impact on the phase difference*, although the phase angle itself is highly susceptible to the couple effect, as shown in (5) and (8). Theorem 1 and the following analysis justify the feasibility of leveraging tag arrays for DOA estimation in the presence of mutual coupling effect.

We designed three experiments to validate the above analysis. The *first* experiment is to measure the phase angle from a tag, while placing another tag next to it at various distances. To assess the interference induced by mutual coupling, we also measure the ground truth phase angle when the second tag is absent. The measured phase errors (i.e., the difference between with or without the second tag) are presented in the upper plot of Fig. 2 for various distances between the two tags. It can be seen from the plot that the phase errors are all quite big until the second tag is placed at a large distance, e.g., 16 cm, from the target tag. Therefore, in order to avoid the large phase interference induced by mutual coupling, the tags should be placed at least 16 cm away from each other.

The *second* experiment is to measure the phase difference by placing the two tags in parallel on the same plane at various distances. The experiment is conducted as illustrated in Fig. 3. In the first part of the experiment, we place Tag 1 at each of the locations, which are separated 2 cm apart. The phase angles from Tag 1 is measured at each of these locations. Then the ground truth phase difference is calculated by subtracting the phase angle at the left-most position from that measured at any other locations. This approach allow us to obtain the phase differences at various tag-tag distances without the mutual coupling effect. In the second part of the experiment, two tags are deployed: Tag 1 is fixed at the left-most location, while Tag 2 is put at each of the other locations. The phase differences under mutual coupling is then measured different tag-tag distances and are plotted in the lower plot of Fig. 2. It can be seen that the phase difference errors are all smaller than 0.1 radian except when the distance is 10 cm. The phase difference errors are mainly due to the multipath effect and random noise; the impact of mutual coupling on phase difference is

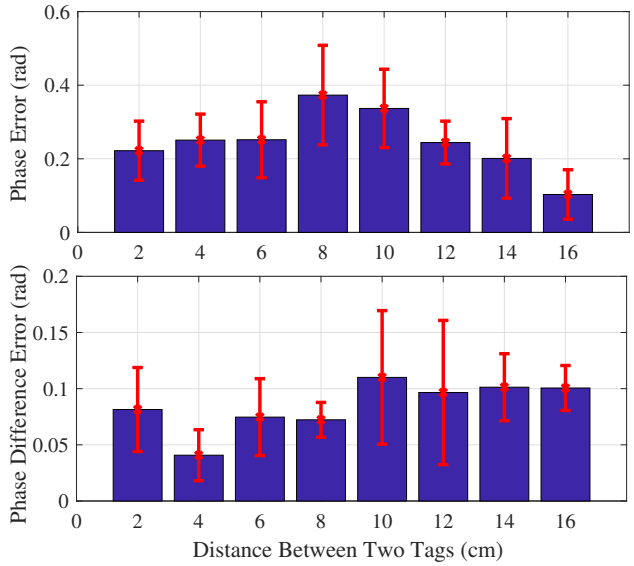

Fig. 2. Impacts of mutual coupling on measured phase angle (the upper plot) and phase difference (the lower plot).

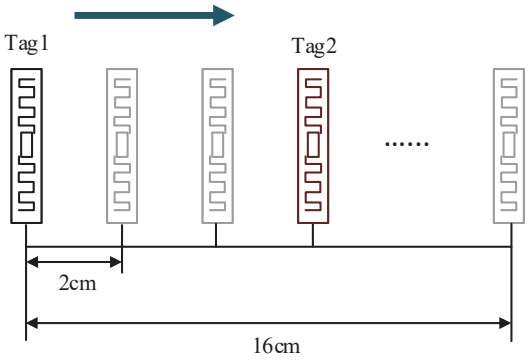

Fig. 3. The setup of the second experiment for assessing the impact of mutual coupling on measured phase difference.

much weaker than the case of phase angles. This experiment validates Theorem 1.

It is worth noting that the above two experiments are different from the Tagyro scheme [9], where the change of phase difference is measured when a tag rotates around another fixed tag. The relative orientation of the pair of tags has a big impact on the mutual impedance. Thus the mutual coupling effect of Tagyro varies with the different rotation angles of the tags. Due to this reason, Tagyro requires careful calibration with a hologram-based approach in order to translate phase offset into the tag array's orientation.

Due to the imperfections in tag production, the impedance of different tag could still be different even if the tags are of the same type and produced by the same manufacturer. We design the *third* experiment to assess the impact of different tag types and different tags of the same type on phase difference measurement. Specifically, we repeat the same experiment with three different types of tags and three different groups of tags of each type. The average phase difference error is summarized in Table 1. It can be observed from the table that, although tags used in each group are of different types, the phase difference error of each group are similar. This experiment validates that the effect of imperfect tag production is negligible on phase difference measurements.

TABLE 1
Impact of Different Types of Tags on Phase Difference Error

Type of RFID tag	Group A	Group B	Group C
ALN-9740	0.08 rad	0.06 rad	0.08 rad
SMARTRAC DogBone	0.11 rad	0.08 rad	0.09 rad
SMARTRAC ShortDipole	0.08 rad	0.07 rad	0.07 rad

2.2.2 *Impact on the Success Rate of Sampling*

Consider, for example, a ULA tag array. The reader keeps on interrogating the tags in the array for a certain period of time. Let n_i be the number of phase angle samples read from tag i in the array. The *success rate of sampling* of tag i is defined as the ratio of n_i over the maximum number of samples collected from any of the tags in the ULA, i.e.,

$$\xi_i = \frac{n_i}{\max_i\{n_i\}}. \tag{10}$$

To measure the mutual coupling effect on tags' success rate of sampling, let P_r denote the received power at the reader, given by [22]

$$P_r = \left(\frac{\lambda}{4\pi l}\right)^4 P_r G_r^2 G_t^2 \frac{4R_A^2}{(R_L+R_A)^2+(X_L+X_A)^2}, \tag{11}$$

where P_r is the reader's transmit power, G_t and G_r are the antenna gains of the tag and the reader, respectively, R_A and X_A are tag antenna's radiation resistance and reactance, respectively, and R_L and X_L are tag chip's radiation resistance and reactance, respectively. To get a valid sample, the received power P_r should exceed the detection threshold P_{th}, i.e., $P_r \geq P_{th}$ [22]. Otherwise, the tag cannot be detected by the reader.

Theorem 2. *Assume the tag chip's impedance R_L is constant. If the tag antenna and chip's reactance satisfy $X_A = -X_L$, the received power at the reader P_r will be an increasing function of R_A when the tag-reader distance l is fixed.*

Proof. If the tag antenna's and chip's reactances satisfy $X_A = -X_L$ (assuming perfect tag production), we have from (11) that

$$P_r = \left(\frac{\lambda}{4\pi l}\right)^4 P_r G_r^2 G_t^2 \frac{4}{(R_L/R_A+1)^2}.$$

It can be easily verify that the received power P_r is an increasing function of R_A, when all other parameters are fixed. □

When the two tags are placed closer, the tag antenna's radiation resistance R_A will become smaller due to the mutual coupling effect [22]. According to Theorem 2, the reader's received power will be lower if the two tags are placed closer to each other. On the other hand, with mutual coupling, $(X_A+X_L)^2$ will not be zero anymore [22], which also reduces the received power as given in (11). In the tag array, mutual coupling could reduce the received powers of some tags, leading to a low success rate of sampling for such affected tags.

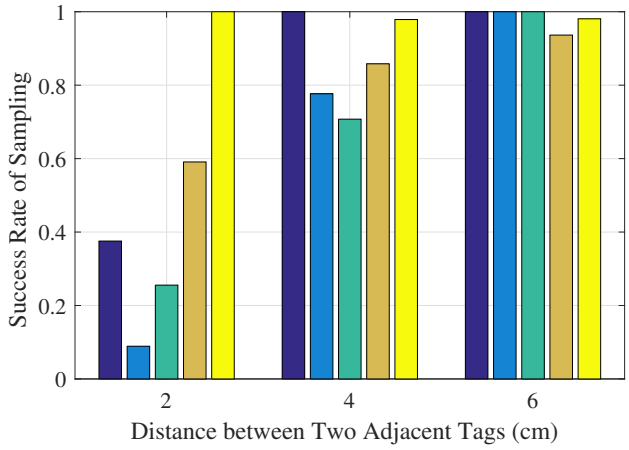

Fig. 4. Impact of mutual coupling on the success rate of sampling, when five tags are placed at 2 cm, 4 cm, and 6 cm intervals.

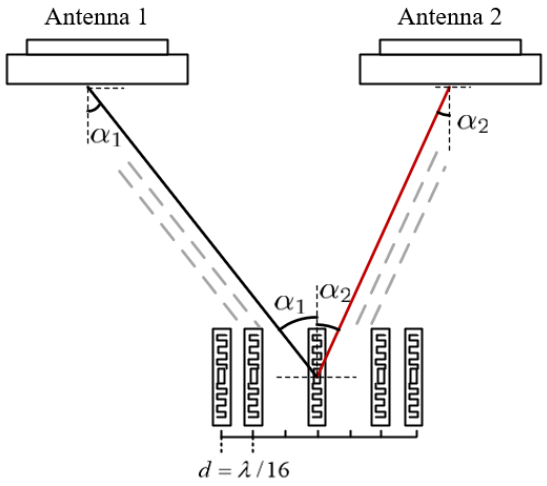

Fig. 5. An overview of the proposed SparseTag system, comprising of a sparse tag array and a reader with two antennas. The antenna locations are known and the center of the tag array is to be localized.

Fig. 4 presents the success rates of sampling of a ULA comprising five tags, placed at 2.1 m away from the reader antenna. We find that the success rates of sampling of all the tags are over 90% when the distance between tags is 6 cm, and the success rates of sampling of all tags are higher than 70% at a 4 cm tag intervals. However, when the tags are placed at 2 cm apart, the success rate of sampling of Tag 2 becomes lower than 10%. That is, this tag cannot be effectively detected on most channels, which generally happens for a tag placed at the center of the ULA, because the mutual coupling effect caused by the tags on both sides are strong. To ensure that all tags in the array be effectively sampled by the reader, the density of the tag array should not be too high. This observation motivates us to design a sparse array for localization.

3 The SparseTag System

3.1 Overview

Fig. 5 provides an overview of the proposed SparseTag system, where an RFID tag array and a reader with two antennas are utilized. We assume the position of the tag array is unknown (i.e., to be detected), while the locations of the two reader antennas are know a priori. The main idea of the SparseTag design is to utilize a sparse tag array to detect the DOAs at the center of the array from both antennas. Then the position of the center of the array will be solved from the known locations of the two antennas and the estimated DOA values.

In typical applications, the tag array is attached to, or even woven into, a small object (e.g., a book, a tablet, or a shirt). The key challenge in the design of SparseTag is how to accurately estimate the DOAs by leveraging the sparse tag array. With a traditional ULA, the sensor element spacing should be smaller than half of the wavelength, while the MUSIC algorithm can be applied to estimate the DOA [17]. As discussed in Section 2, a ULA may not be suitable for positioning a small object. This is because for RFID systems operated in the 900 MHz band, half of a wavelength is already 16 cm. Furthermore, with an N-element ULA, the MUSIC algorithm only estimates up to $(N-1)$ DOAs. Usually spatial smoothing is adopted to decorrelate uncorrelated sources, which takes half of the elements and consequently, the maximum number of estimated DOAs will be halved [23]. In this paper, a novel sparse RFID tag array structure is proposed to achieve high success rate of sampling for the tags in the array, while the minimum spacing of the tags can be as small as $\lambda/16$. Since usually a tag, e.g., an ALN-9740 tag, is about 1 cm wide, the minimum spacing of the tags should be no smaller than 1 cm such that the tags will not overlap with each other. Consequently, the minimum spacing of the proposed array structure is set to $\lambda/16$, which is roughly 2 cm for the 900 MHz band. Moreover, we derive the difference co-array of the sparse tag array, which can provide a higher DOA resolution for more accurate localization performance.

The proposed SparseTag system mainly comprise four modules, i.e., (i) Sparse Array Processing, (ii) Co-array Design, (iii) DOA Estimation, and (iv) Location estimation. We describe the design of each of the modules in the following.

3.2 Sparse Array Design

In order to adopt tag arrays to localize small objects, the number of tags, as well as the tag spacing, cannot be too big. To address these issues, we propose to adopt a sparse array that comprises of N tags with a nonuniform linear placement, which is quite different from the traditional ULA plus MUSIC approach [17].

Let the steering vector for direction α be denoted by $\vec{a}(\alpha)$, with elements $\exp\{j\frac{2\pi}{\lambda}d_i \sin\alpha\}$, where d_i is the location of tag i and λ is the wavelength of the carrier frequency. Assume there are D multipath components from the propagation environment, each having direction α_i and power σ_i^2, $i = 1, 2, ..., D$. The received signal at time t can be written as

$$\vec{g}[t] = \sum_{i=1}^{D} \vec{a}(\alpha_i)s_i[t] + \vec{n}[t] = \mathbf{A}\vec{s}[t] + \vec{n}[t], \qquad (12)$$

where $\mathbf{A} = [\vec{a}(\alpha_1), \vec{a}(\alpha_2), ..., \vec{a}(\alpha_D)]$ denotes the array manifold matrix, $\vec{s}[t] = [s_1[t], s_2[t], ..., s_D[t]]^T$ denotes the

source signal vector, and $\vec{n}[t]$ is the additive white noise vector. Assuming the multipath components are temporally uncorrelated, the source autocorrelation matrix will then assume a diagonal structure. Considering the second-order information of the received signal $\vec{g}(t)$, its covariance matrix, denoted by $\mathbf{R}_{gg}$, can be derived as

$$\begin{aligned}\mathbf{R}_{gg} &= \mathbb{E}[\vec{g}(t)\vec{g}(t)^H] = \mathbf{A}\mathbf{R}_{ss}\mathbf{A}^H + \sigma_n^2\mathbf{I} \\ &= \sum_{i=1}^{D}\sigma_i^2\vec{a}(\alpha_i)\vec{a}(\alpha_i)^H + \sigma_n^2\mathbf{I}.\end{aligned} \tag{13}$$

We next vectorize the $\mathbf{R}_{gg}$ in (13) to derive the measurement vector, which is given by

$$\begin{aligned}\vec{z} &= \text{vec}(\mathbf{R}_{gg}) = \text{vec}\left[\sum_{i=1}^{D}\sigma_i^2\vec{a}(\alpha_i)\vec{a}(\alpha_i)^H\right] + \sigma_n^2\vec{1}_n \\ &= (\mathbf{A}^* \odot \mathbf{A})\vec{p} + \sigma_n^2\vec{1}_n,\end{aligned} \tag{14}$$

where $\vec{p} = [\sigma_1^2, \sigma_2^2, ..., \sigma_D^2]^T$, $\vec{1}_n = [\vec{e}_1^T, \vec{e}_2^T, ..., \vec{e}_N^T]^T$, and $\vec{e}_i$ is a column vector whose ith element is "1" and all other elements are "0." Here the measurement vector is regarded as the signal received at an array with a manifold of $(\mathbf{A}^* \odot \mathbf{A})$ [24], where $\odot$ represents the Khatri-Rao (KR) product. The matrix $(\mathbf{A}^* \odot \mathbf{A})$ can be regarded as the manifold of a longer array, whose antenna positions are determined by the different values in the set $\{\vec{x}_i - \vec{x}_j\}$, $1 \le i$ and $j \le N$, where $\vec{x}_i$ is the location vector of Tag i. This new array is termed the *difference co-array* [24]. In SparseTag, DOA is estimated with the difference co-array, which effectively exploits the second-order statistics of the signal for an increased DOF.

3.3 Difference Co-array Design

In the following, we first present several basic definitions related to the difference co-array. We then present the design of the difference co-array for the sparse tag array used in SparseTag.

3.3.1 Definitions

Definition 1. *(Difference Co-Array). Consider a sparse, N-element tag array. Let $\vec{x}_i$ be the location vector of Tag i. The difference co-array of the sparse array is defined as [24]*

$$\mathcal{D} = \{\vec{x}_i - \vec{x}_j, 1 \le i, j \le N\}. \tag{15}$$

The difference co-array can be regarded as a new array, where the tags are placed at the locations given in the set $\mathcal{D}$. In addition, the values of the cross correlation elements in the covariance matrix of the received signal by the sparse tag array are determined by the number of elements in the difference co-array, which is helpful to improve the number of estimated DOAs.

Definition 2. *(Restricted Array). A sparse, N-element tag array is a restricted array if its difference co-array is hole-free [25].*

If the difference co-array is hole-free, it is also a ULA. Therefore, the traditional subspace based MUSIC algorithm can be employed to estimate DOA using a hole-free difference co-array. For instance, the tags are placed at the positions given by the set S, which is given by

$$\mathcal{S} = \{m \cdot d,\ m = 1, 2, 4\}. \tag{16}$$

where d is the minimum spacing between tags. The corresponding difference co-array can be derived as

$$\mathcal{D} = \left\{-\vec{3}, -\vec{2}, -\vec{1}, \vec{0}, \vec{1}, \vec{2}, \vec{3}\right\}. \tag{17}$$

Although the position $3d$ is missing in this sparse array (see (16)), there is no missing vector in the difference co-array set $\mathcal{D}$ (i.e., it includes all the vectors from $-\vec{3}$ to $\vec{3}$, see (17)). Consequently, this array is still useful for DOA estimation using the MUSIC algorithm.

Definition 3. *(Degree of Freedom (DOF): The DOF of a sparse array is the cardinality of its difference co-array $\mathcal{D}$ [24].*

The DOF of a sparse array can be derived by the cardinality of its difference co-array $\mathcal{D}$, which indicates the maximum number of DOAs that can be estimated.

Definition 4. *(Weight Function). For a sparse, N-element tag array, its weight function $w(\vec{d})$ is defined as the number of tag pairs that can achieve the difference co-array element $\vec{d}$. The weight function is given by [24]*

$$w(\vec{d}) = \left|\left\{(\vec{x}_i, \vec{x}_j) | \vec{x}_i - \vec{x}_j = \vec{d}\right\}\right|,\ \vec{d} \in \mathcal{D}. \tag{18}$$

The weight function indicates the how serious the mutual coupling effect is, which is helpful for our proposed sparse tag array.

3.3.2 Difference Co-array

Assume N is an odd number. Then the tag placement in the N-element sparse tag array are given in the set $\mathcal{S}$, which is

$$\begin{aligned}\mathcal{S} = \{&m \cdot d,\ m = 1, ..., (N+1)/2 - 1, \\ &(N+1)/2 + 1, (N+1)/2 + 3, ..., N + 2\},\end{aligned} \tag{19}$$

where the tag minimum spacing is set to $d = \lambda/16$; such small spacing allows us to use a small-sized tag array to localize small objects. The proposed sparse tag array has a symmetric structure; its left and right halves have the same tag spacing arrangement. In addition, the gaps from the two tags placed at positions $(\frac{N+1}{2} - 1)d$ and $(\frac{N+1}{2} + 3)d$ to the tag placed at the center of the array (i.e., at position $(\frac{N+1}{2} + 1)d$) is both $2d$. Thus the proposed array is a sparse array.

The sparse tag array used in SparseTag has the following three key advantages. First, its symmetric structure helps to suppress the mutual coupling effect, which usually limits the performance of traditional tag arrays. The reduced mutual coupling leads to less interference in measured phase difference and thus, higher accuracy in the estimation of DOAs. Second, the sparse structure also helps to mitigate the degradation of the success rate of sampling of the tags in the array, specifically, the tag at the center of the array. Third, it allows us to use tag arrays with a smaller physical dimension. Such smaller-sized tag arrays help to improve the DOA resolution and are easier to deploy, such as attached to small objects or woven into clothing.

The difference co-array corresponding to the proposed sparse array is given by the following placement set S_d.

$$\mathcal{S}_d = \{m \cdot d,\ m = -(N+1), -N, ..., N, (N+1)\}. \tag{20}$$

Theorem 3. *The proposed sparse array is a restricted array. That is, it is a hole-free difference co-array.*

Proof. The difference co-array of the proposed sparse array is a ULA. It is easy to verify that it is a hole-free difference co-array, with the given placement set $\mathcal{S}_d$. Thus we conclude that it is a restricted array. □

Corollary 3.1. *The proposed sparse array's co-array is the same as that of an* $(N+2)$ *ULA.*

Proof. The proposed sparse array has the same left-most and right-most tag positions at d and $(N+2)d$, respectively, as that of an $(N+2)$ ULA. In addition, both arrays are restricted arrays. Therefore, we conclude that the proposed sparse array has the same co-array as that of the $(N+2)$-element ULA. □

Theorem 4. *The DOF of the sparse* N*-element array is* $2N+3$.

Proof. The proposed sparse array is given by the position set $\mathcal{S}$, and the cardinality of its difference co-array $\mathcal{S}_d$ is $2N+3$. Therefore we conclude that the DOF of the sparse array is $2N+3$ according to Definition 3. □

Theorem 5. *The weight function of the proposed* N*-element sparse array is* $w(\vec{d}=\vec{0})=N$ *and* $w(\vec{d}=\vec{1})=N-3$.

Proof. When $\vec{x}_i = \vec{x}_j$, we have the case $\vec{d}=\vec{0}$. This case occurs N times for an N-element array, i.e., when $i=j=1,2,...,N$. Therefore we have $w(\vec{d}=\vec{0})=N$ according to Definition 4.

Furthermore, consider two different subarrays given by sets $\mathcal{S}_l = \{m\cdot d, m=1,2,...,\frac{N+1}{2}-1\}$ and $\mathcal{S}_r=\{m\cdot d, m=\frac{N+1}{2}+3, \frac{N+1}{2}+4,...,N+2\}$, respectively. The case $\vec{d}=\vec{1}$ takes place for $(\frac{N+1}{2}-2)$ times in each subarray. Furthermore, for the subarray given by set $\mathcal{S}_c=\{m\cdot d, m=\frac{N+1}{2}-1, \frac{N+1}{2}+1, \frac{N+1}{2}+3\}$, the case $\vec{d}=\vec{1}$ does not arise at all. It follows that $w(\vec{d}=\vec{1})=(\frac{N+1}{2}-2)*2=N-3$. □

We make the following observations from the above theorems and corollary.

- The proposed N-element sparse array has the same DOF as an $(N+2)$-element ULA. Using the proposed sparse array, we can achieve a higher maximum number of estimated DOAs than using a ULA with the same amount of tags and the MUSIC algorithm.
- Using the proposed sparse array can achieve a higher sampling rate of the tags. This is because its weight function, i.e., $w(\vec{d}=\vec{1})=N-3$, is smaller than that of an $(N+2)$-element ULA. In Fig. 6, we compare a 7-tag ULA with a 5-tag proposed sparse array. In each figure, the upper plot shows the placement of the tags, while the lower plot presents the corresponding weight function $w(n)$. It can be seen that the 5-tag sparse array has the same DOF, i.e., 13, as the 7-tag ULA, since they share the same difference co-array. Furthermore, it shows that $w(\vec{1})=2$ for the 5-tag sparse array and $w(\vec{1})=6$ for the 7-tag ULA.
- There are other types of sparse arrays, e.g., the co-prime array [26], nested array [24], and super nested array [27], which can also achieve a larger DOF than the proposed sparse array. However, such arrays may not be suitable for the deployment of tag arrays. This is because such arrays all require a relatively larger physical space, which may not be available for small objects. Moreover, such arrays' structures are not symmetric. Therefore, they may incur more serious mutual coupling among the tags, leading to large interference in the RFID phase and phase difference samples.

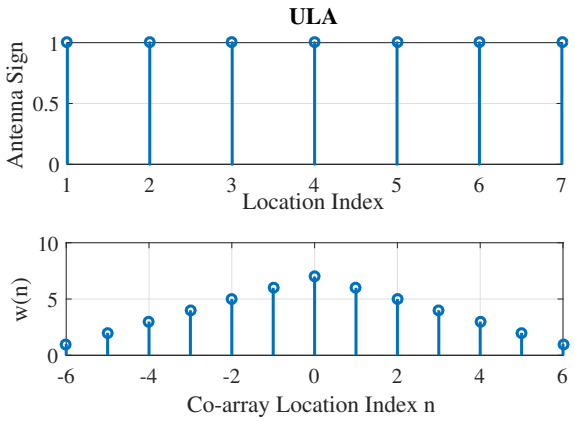

(a) A 7-tag ULA and its weight function $w(n)$. Upper: antenna sign is 1 means a tag is placed at the corresponding location; Lower: the weight function.

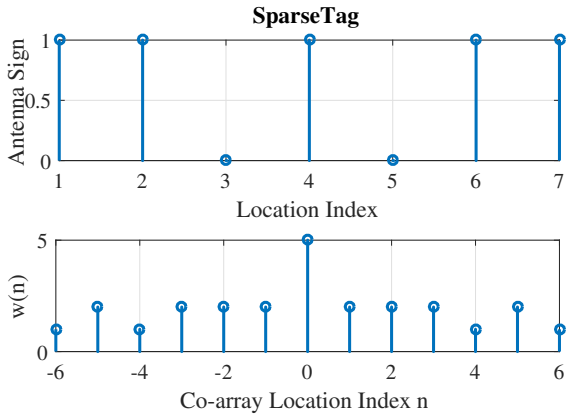

(b) A 5-tag sparse array and its weight function $w(n)$. Upper: antenna sign is 1 means a tag is placed at the corresponding location; Lower: the weight function.

Fig. 6. A 7-tag ULA versus a 5-tag sparse array.

3.4 Estimation of DOA

The difference co-array of the proposed sparse array is then leveraged for DOA estimation. A spatial smoothing based method is employed, which is different from the existing approach that utilizes spatial smoothing to mitigate correlated sources [24]. The SparseTag approach constructs an observation matrix for the difference co-array, which does not require using high-order cumulative signals.

Specifically, we first derive the array manifold $(\mathbf{A}^*\odot\mathbf{A})$ following (14), which has a dimension $N^2\times D$. According to Theorem 4, we next construct a matrix $\mathbf{B}$ with dimension $(2N+3)\times D$ by removing the repeated rows from the array manifold. Next, we sort this constructed matrix to ensure that row i corresponds to the tag position $(-N-1+i)d$

in the proposed difference co-array. Then we obtain a new vector $\vec{y}$, which is written as

$$\vec{y} = \mathbf{B}\vec{p} + \sigma_n^2 \vec{e}, \tag{21}$$

where $\vec{e} \in \Re^{(2N+3)\times 1}$ is a vector whose $(N+1)$th element is "1" and all other elements are "0."

Following the placement set (20), we divide the co-array into $(N+1)$ overlapping subarrays, each having $(N+1)$ elements, while the ith subarray is given by the following placement set:

$$\mathcal{S}(i) = \{(-i+1+m)\cdot d,\ m = 0, 1, ..., N\}. \tag{22}$$

Let $\vec{y}(i)$ be a new vector for subarray i that comprises the same elements of $\vec{y}$ ranging from the $(N+1-i+1)$th element to the $(2N+1-i+1)$th element:

$$\vec{y}(i) = \mathbf{B}(i)\vec{p} + \sigma_n^2 \vec{e}(i), \tag{23}$$

where $\mathbf{B}(i)$ is a matrix with dimension $(N+1)\times D$, comprising the same rows of $\mathbf{B}$ ranging from the $(N+1-i+1)$th row to the $(2N+1-i+1)$th row; and $\vec{e}(i)$ is a vector whose ith element is "1" and all other elements are "0." Consequently, the spatially smoothed matrix $\mathbf{R}_s$ is obtained as

$$\mathbf{R}_s = \frac{1}{N+1}\sum_{i=1}^{N+1} \vec{y}(i)\vec{y}(i)^H. \tag{24}$$

We then utilize $\mathbf{R}_s$ to estimate DOA. With our approach, N DOAs can be estimated, which is considerably larger than what can be obtained with the MUSIC plus ULA approach (i.e., $(N-1)/2$). SparseTag incorporates a directional antenna for increased range. The line-of-sight (LOS) component is dominant and a strong incident wave. The proposed sparse array can achieve a higher angle resolution than the existing approach.

3.5 Location Estimation with DOAs

The proposed SparseTag system comprises a tag array and a reader with two directional antennas, each of which operates on 50 channels in the 900 MHz band and samples phase angle of the received tag response. Some channel information may not be reliable due to the multipath propagation.

Fig. 7 presents the phase angles collected from a five-tag sparse array from the 50 channels. It can be seen the phase difference of two adjacent tags on most channels are similar. This is due to the small distance between the pair of tags (e.g., 2 cm or 4 cm); and the 0.5 MHz change of channel frequency caused by channel hopping can hardly cause a sufficient change in phase. We also find from Fig. 7 that the phase difference collected from some channels are highly different from others. Such difference is caused by the multipath effect on different channels. Some channels are more susceptible to the multipath effect; so the phase angles collected from such channels should be filtered out before DOA estimation.

To address this issue, SparseTag adopts a channel selection procedure. Denote $\phi_{(i,f_m)}(t)$ as the phase angle sampled from Tag i on channel f_m at time t. The phase difference between Tag i and Tag $i+1$ at time t, denoted by $\Delta_{(i,f_m)}(t)$, is given by

$$\Delta_{(i,f_m)}(t) = \phi_{(i+1,f_m)}(t) - \phi_{(i,f_m)}(t),\ i = 1, 2, ..., N-1. \tag{25}$$

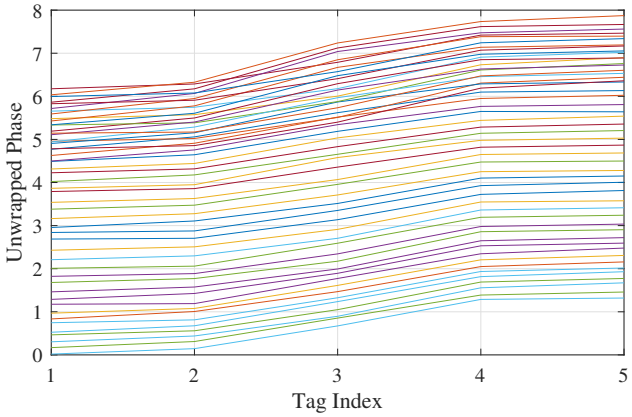

Fig. 7. Phases angles sampled from a 5-tag sparse array over 50 channels (each line corresponds to a different channel).

We select the medium value of all the phase differences from all the channels for robustness, since in many cases only a few channels are impaired. After selecting the right channel, we recalculate the phase angles of all the tags in the array. Using the Tag 1 phase angle as a reference and assuming $\phi_{(1,f_m)}(t) = 0$ at time t, the phase value of Tag i is

$$\phi_{(i,f_m)}(t) = \phi_{(i-1,f_m)}(t) + \Delta_{(i-1,f_m)}(t),\ i = 2, 3, ..., N. \tag{26}$$

The received signal is next reconstructed as

$$\hat{g}(t) = [e^{(j(2\pi - \phi_{(1,f_m)}(t)))}, ..., e^{(j(2\pi - \phi_{(N,f_m)}(t)))}]. \tag{27}$$

Note that we have the terms $(2\pi - \phi_{(i,f_m)}(t))$ in (27) due to the reader operation of the phase angle. Two DOAs are estimated using multiple snapshots of received signal (each comprising samples from all the 50 channels and each tag), one for each reader antenna. In Fig. 8, we plot the power spectrum density obtained by SparseTag and ULA arrays from the same experimental setting. The ground truth of DOA is marked by the red vertical line in the figure, which indicates 28°. Fig. 8 shows that the peak of the SparseTag curve is considerably sharper and closer to the ground truth than the peak of the ULA curve obtained using the MUSIC algorithm. DOA estimation with SparseTag is more accurate than with ULA, because SparseTag achieves larger DOFs than ULA.

The center of the tag array can be derived from the two estimated DOAs and the known coordinates of the two antennas. Consider a coordinate system where the direction of the tag array is the x-axis and the y-axis be perpendicular to the tag array. Assume (x_i, y_i) is the known coordinates of antenna i, $i = 1, 2$, and let (x_c, y_c) denote the coordinates of the center of the tag array. The two DOAs and the coordinates satisfy the following conditions (see Fig. 5).

$$\cot(\alpha_1) = \frac{y_c - y_1}{x_c - x_1}, \quad \cot(\alpha_2) = \frac{y_c - y_2}{x_c - x_2}. \tag{28}$$

The cotangent function in (28) is given by $\cot(\alpha) = \cos(\alpha)/\sin(\alpha)$. We solve (28) for the coordinates of the

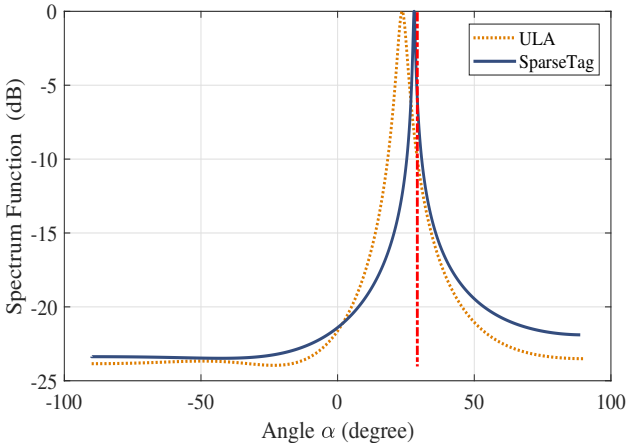

Fig. 8. DOA estimation results obtained using SparseTag and ULA. The red vertical dashed line marks the ground truth of 28°.

center of the RFID tag array (x_c, y_c), which is given by

$$x_c = \frac{x_1 \cot(\alpha_1) - x_2 \cot(\alpha_2) + y_2 - y_1}{\cot(\alpha_1) - \cot(\alpha_2)} \tag{29}$$

$$y_c = \frac{(x1 - x2)\cot(\alpha_1)\cot(\alpha_2) + y_2 \cot(\alpha_1) - y_1 \cot(\alpha_2)}{\cot(\alpha_1) - \cot(\alpha_2)}. \tag{30}$$

4 Experimental Validation

4.1 System Implementation and Experiment Setup

We develop an implementation of SparseTag using an commodity Impinj R420 RFID reader equipped with two circular polarized antennas and different types of RFID tags. When scanning the tags, the reader hops among 50 channels in the range of 902.5 MHz to 927.5 MHz, as required by the FCC. A Lenovo Thinkpad S3 laptop is used to control the reader and process the collected data. The RFID reader samples channel related data from received tag responses such as time stamp, phase angle, RSSI, and Doppler shift using a Low-level Reader Protocol (LLRP) [18]. Furthermore, we build the RFID tag arrays using three different types of passive tags, including ALN-9740, SMARTRAC DogBone, and SMARTRAC ShortDipole.

Extensive experiments are conducted in two different environments, including a 7.5×5.6 m^2 computer laboratory and an 8×2.4 m^2 anechoic chamber, which are illustrated in Fig. 9. The computer lab is a more cluttered environment with computers and furniture, which cause the multipath propagation of RFID signals. We also try to introduce more severe multipath effect by placing chairs in the LOS path between the tag array and antennas. In the anechoic chamber setup, most multipath effects are eliminated due to the special absorbing material mounted on the wall, ceiling, and floor. In the experiments, we mark various positions on the floor, which are considered as ground-truth. The tagged object (e.g., a book) is hold by an easel to be in the same horizontal plane as the two reader antennas. As discussed, the target of localization is the center of the tag array. The same experiments are conducted using the ULA tag array with identical hardware and environment setup to assess the strengths of the proposed sparse tag array.

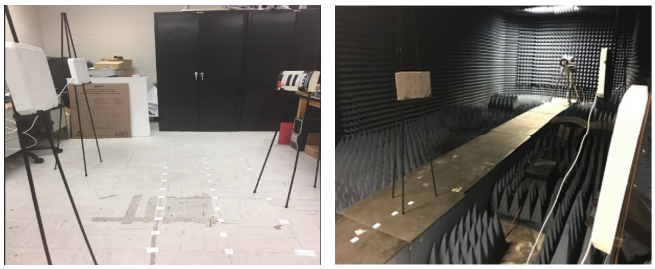

(a) The computer lab setup. (b) The anechoic chamber setup.

Fig. 9. The setup of two experimental scenarios for SparseTag performance evaluation.

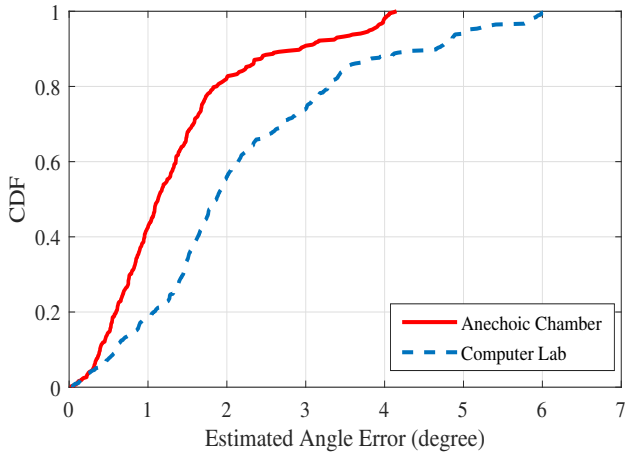

Fig. 10. CDFs of DOA errors achieved by SparseTag with a 5-tag sparse array in the computer lab and anechoic chamber scenarios.

4.2 Evaluation in Different Localization Scenarios

We conduct experiments in both the lab and anechoic chamber environments. In Fig. 10 and Fig. 11, we plot the cumulative distribution function (CDF) of the DOA and location errors obtained by SparseTag with a 5-tag sparse array. The median error of DOA estimation in the anechoic chamber scenario is $1.125°$, while the median error in the computer lab scenario is $1.872°$. Fig. 10 also shows that the maximum error in anechoic chamber is only $4.024°$. The angle estimation accuracy is higher when the system is tested in the anechoic chamber than the computer lab experiments, because the multipath effect is eliminated in the anechoic chamber setup. Fig. 11 also shows that the location error in the anechoic chamber scenario is smaller than that in the computer lab scenario. The median location error in the anechoic chamber environment is 3.419 cm, and the median location error in the computer lab environment is 5.012 cm.

To validate the performance of SparseTag in an environment with stronger multipath effect, we place some chairs as obstacles in the LOS path between the tag array and the reader antennas. The mean localization errors of all the three scenarios are plotted in Fig. 12, where both the SparseTag errors and the ULA errors are provided. It is shown in the figure that, the mean estimation error of the 5-tag SparseTag array in the rich multipath environment is 5.637 cm, while the mean error in the typical Computer Lab environment is 5.158 cm. For the 5-tag ULA array, the errors

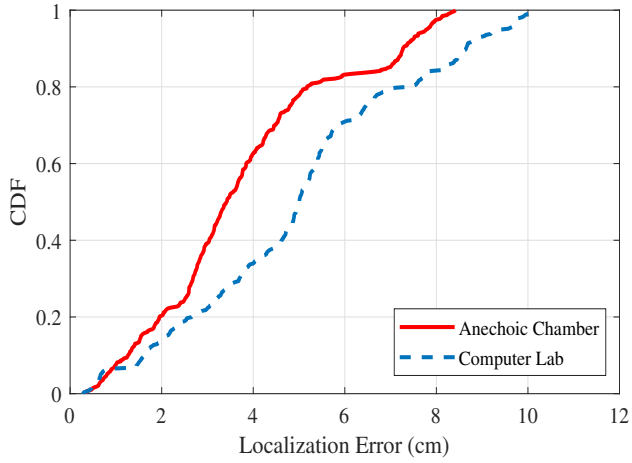

Fig. 11. CDFs of localization errors achieved by the 5-tag SparseTag in the computer laboratory and anechoic chamber scenarios.

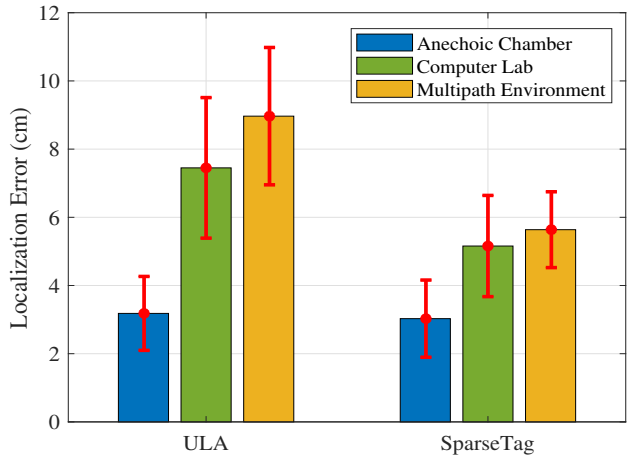

Fig. 12. Mean localization errors achieved by the 5-tag ULA array and SparseTag array in three different scenarios.

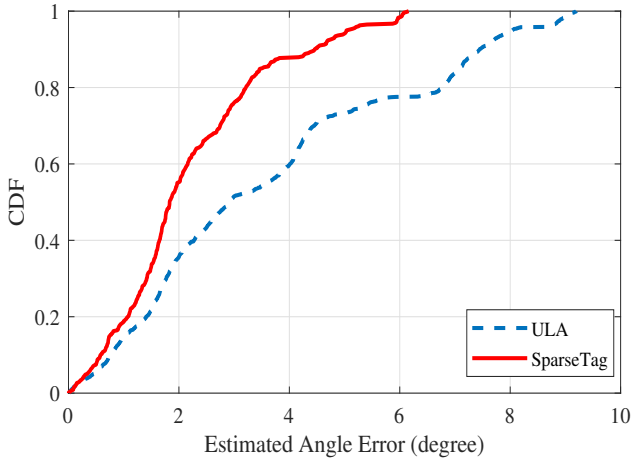

Fig. 13. CDFs of DOA errors achieved by a 5-tag SparseTag and a 5-tag ULA in the computer lab experiment.

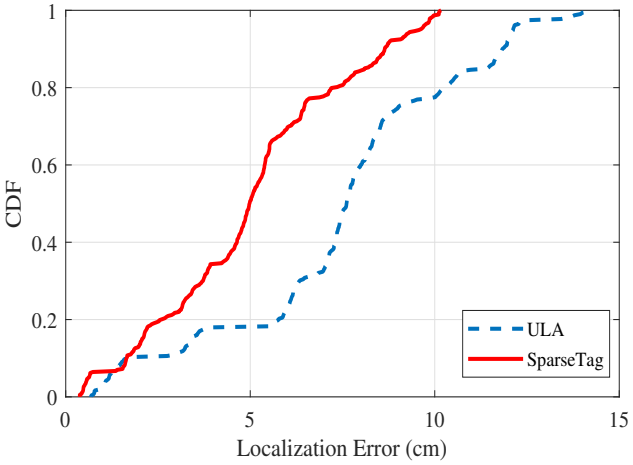

Fig. 14. CDFs of localization errors achieved by a 5-tag SparseTag and a 5-tag ULA in the computer lab experiment.

in the same environments increase to 8.967 cm and 7.450 cm, respectively. These results validate that the proposed spare array is more robust to the multipath effect than the ULA array with the same number of tags.

4.3 Comparison with Baseline Scheme

To validate the strengths of the proposed sparse tag array, we conduct more experiments to compare SparseTag with the traditional ULA plus MUSIC localization system [10], [17]. Fig. 13 presents a comparison of SparseTag with ULA in the computer lab environment. The CDFs of DOA errors obtained with a 5-tag ULA and a 5-tag SparseTag systems are plotted. We find that the maximum estimated DOA error of ULA is $9.198°$, while the maximum DOA error of SparseTag is $6.161°$. The median errors for ULA and SparseTag are $2.909°$ and $1.831°$, respectively. In addition, 90% of SparseTag estimated DOA errors are below $5°$. We conclude that SparseTag is more accurate for DOA estimation than ULA, because SparseTag achieves a higher angle resolution than ULA. With the spatially smoothed matrix $\mathbf{R}_s$ in (24), the number of estimated DOAs is more than that of ULA with the same number of tags, which means the sparse tag array performs better in rich multipath environments than the ULA array.

Fig. 14 presents the CDFs of localization errors obtained with the 5-tag SparseTag and 5-tag ULA. The same localization estimation method is used with the two different tag arrays in the same environment. We find that the median error of SparseTag is 4.985 cm, while the median error of ULA is 7.611 cm. Usually an UHF passive tag is about 10 cm long. For instance, the ALN-9740 tag used in our experiments is 98.2 mm $\times$ 12.3 mm. The SparseTag's median error is about half of the tag length; therefore it is sufficiently accurate for many practical applications. Fig. 14 also shows that the maximum error of SparseTag is 10.114 cm, which is much smaller than the ULA's maximum error. Thus it is validated that SparseTag can achieve a higher accuracy of localization than ULA.

We also compare the proposed system with an existing RFID tag array based localization technique using a mobile antenna [12] in the same rich multipath environment where the results in Fig. 12 are obtained. Rather than leveraging two antennas, a single mobile antenna is utilized for positioning of 5-tag ULA array and the sparse array. The mean

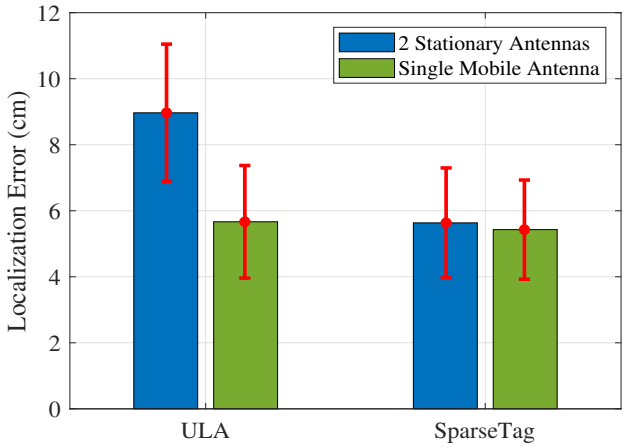

Fig. 15. Mean localization errors obtained by the 5-tag ULA array and the SparseTag array with two stationary antennas and with a single mobile antenna.

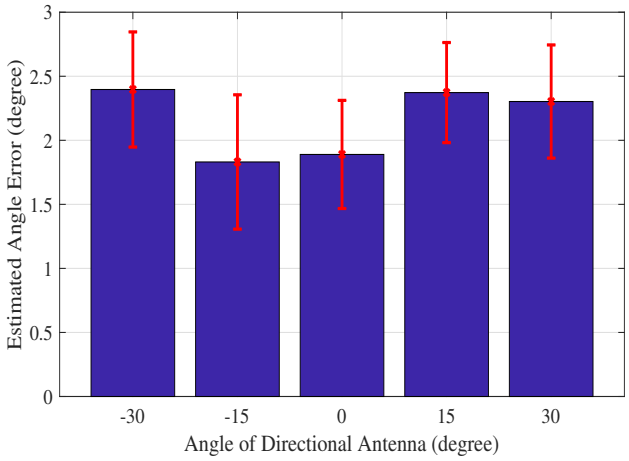

Fig. 16. Impact of the angle of the directional antenna.

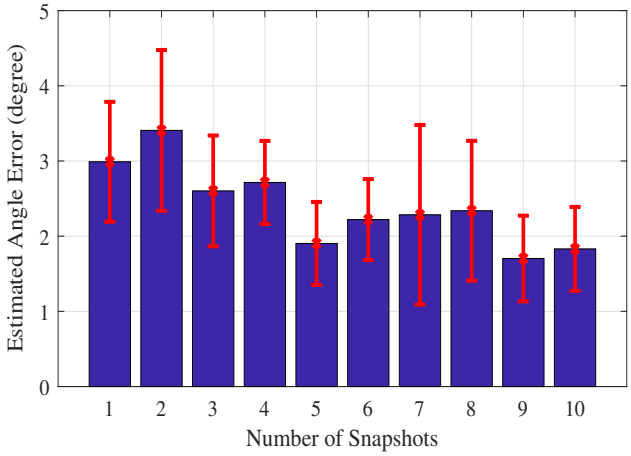

Fig. 17. Impact of the number of snapshots.

estimation errors are presented in Fig. 15. As the figure shows, the ULA's localization error decreases from 8.967 cm to 5.666 cm, when the mobile antenna is leveraged in the system. This is because, the mobile antenna can be considered as multiple virtual antennas, which help to mitigate the multipath effect. However, for SparseTag, the improvement in accuracy brought about by the use of the mobile antenna is not obvious. This experiment result indicates that the multipath effect has already been effectively mitigated by using the proposed 5-tag sparse array, so use of the mobile antenna does not further improve the localization accuracy. We thus conclude that the proposed SparseTag system achieves high accuracy without using moving antennas, making it easier to deploy and more adaptable.

4.4 Impact of System Design Factors

To further assess the proposed system, we conduct more experiments on the influence of several design factors. Since directional antennas are used in our experiments, we also evaluate how the relative angle of the directional antenna affects the estimation results. Fig. 16 shows the estimation errors for different antenna angles, including -30°, -15°, 0°, 15°, and 30°, where 0° means the antenna directly faces the tag array. From Fig. 16, we can see that the estimation errors at different angles are all around 2°, and the error does not increase as the angle of the antenna is changed. This experiment shows that the estimated DOA is not seriously affected by the relative angle of the directional antenna.

We also examine the effect of the number of snapshots on DOA estimation. Recall that each snapshot comprises samples from all the 50 channels and from each tag. Fig. 17 shows that the DOA error obtained by one to 10 snapshots. It can be seen that when there are less than three snapshots, the DOA error is about 3°, while the error remains at about 2° with five or more snapshots. This is because only one or two snapshots cannot effectively remove the white noise in the RFID signals. If the number of snapshots is larger than nine, the effect of noise can be mostly removed using a spatial smoothing based method. As a result, we choose 10 snapshots in our SparseTag system.

Fig. 18 illustrates the impact of the difference between the heights of the reader antennas and the tag array. The height difference is represented by the angle between the horizontal plan and the line connecting the antenna and the center tag, as illustrated in Fig. 19. When the sparse tag array is not on the same horizon plane as the antennas, the DOA estimation error will increase quickly. This is because SparseTag mainly focuses on 2D localization; when the antennas are at a different height from the tag array, an additional phase offset will be introduced. The phase offset is related to the height difference, and so the DOA error will increase as the height difference becomes larger.

Fig. 20 presents the estimated DOA errors obtained using different types of arrays. In our experiments, we evaluate the DOA estimation accuracy of 4 types of tag arrays. The first and the second arrays are ULA with 3 and 5 tags, respectively, while the third and the fourth arrays are sparse tag arrays, which consist of 5 tags at positions (0, d, $3d$, $5d$, $6d$), and 7 tags at positions (0, d, $2d$, $4d$, $6d$, $7d$, $8d$), respectively. From Fig. 20, we can see that the angle errors of ULA are both higher than 3°, while both sparse tag arrays achieve lower errors about 2°. This is because the sparse tag array achieves a higher angle resolution than ULA with the same number of tags. Fig. 20 also shows that the errors of the

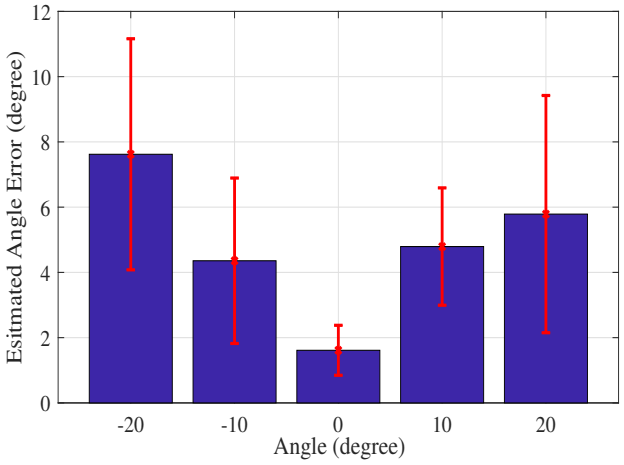

Fig. 18. Impact of the height difference between the tag array and the antennas, which is represented by the angle as shown in Fig. 19.

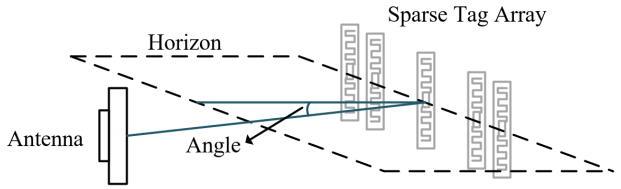

Fig. 19. The height difference between the tag array and the antennas is represented by the angle between the horizontal plan and the line connecting the antenna and the center tag.

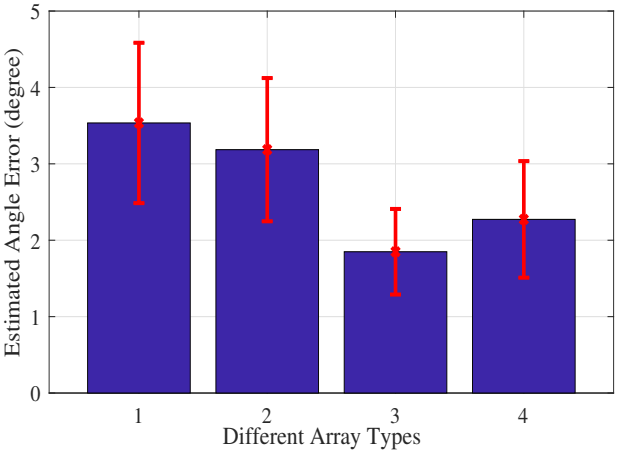

Fig. 20. Impact of different array types on DOA estimation error. The first and second arrays are ULA with 3 and 5 tags, respectively, while the third and fourth arrays are sparse tag arrays, with 5 tags at positions $(0, d, 3d, 5d, 6d)$, and 7 tags at positions $(0, d, 2d, 4d, 6d, 7d, 8d)$, respectively.

5-tag sparse array is close but lower than that of the 7-tag sparse array. The 5-tag sparse array is sufficient to estimate DOA accurately.

4.5 Evaluation of the Near-field Effect

According to the FCC regulation on transmit power, the distance between the reader antenna and the tag array is usually not large. The tag array is placed within 3 m from the polarized antennas in all our experiments. Otherwise, the tag array can hardly be detected by the reader due to extremely weak RSS. The MUSIC algorithm is adopted for DOA estimation, which assumes the incident wave to the array is a plane wave. Such an assumption may not be rigorous in near-field communications scenarios, and will cause extra estimation errors. Fig. 21 shows an antenna and a simple 2-tag array, where the tags are placed d apart from each other. The tag-to-reader distances are L_1 and L_2 for Tag 1 and Tag 2, respectively. Here α_m is the DOA to be estimated. If we assume the incident wave to Tag 1 and the wave to Tag 2 are along two parallel lines (i.e., the plane wave assumption holds true), $(L_1 - L_2)$ can be consider as an edge of the right angled triangle as shown in the figure. Thus α_m can be easily computed as:

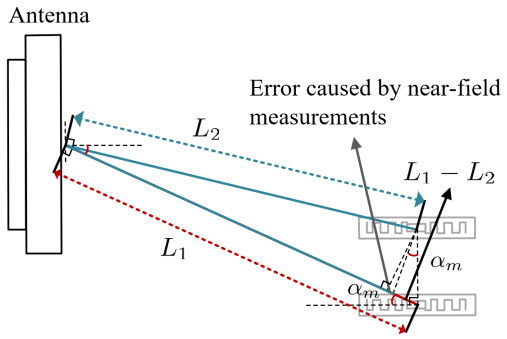

Fig. 21. Illustrate the error introduced by the near-field measurements.

$$\alpha_m = \arcsin\left(d/(L_1 - L_2)\right), \tag{31}$$

where $(L_1 - L_2)$ can be estimated from the phase difference of the two tags. However, when the two tags are close to the antenna, the two incident waves will not be parallel and the relationship (31) will not hold true, which leads to additional DOA errors.

To evaluate the influence of such near-field effect, we conduct two experiments to find out the effective range of the SparseTag system. We first test the influence of the distance between the tag array and the antennas. We estimate DOAs under different tag-to-reader distances, ranging from 0.5 m to 2.5 m, and the results are presented in Fig. 22. We find that when the distance is 0.5 m or lower, the DOA error will be higher than 3.6°. When the distance is 1 m or larger, the DOA error will be lower than 3°. These results show that the influence of the tag-to-antenna distance is not strong since in typical applications the tag array will placed more than 1 m away from the antenna.

The second experiment examines the influence of different measuring angle on DOA error. We place the tag array at a fixed distance (e.g., 2 m) from the reader, and estimate the DOA from different relative antenna-tag array positions, where the ground truth DOA ranges from $-75°$ to $75°$. The estimation errors are presented in Fig. 23. We find that the DOA error is lower than $3.5°$ when the tag array is place between $-60°$ and $60°$. However, the error becomes considerably large when the DOA is over $75°$. This is because when the angle is too large, the polarized antenna can hardly collect phase values from all the channels and from each tag in the array. From these two experiments, we conclude that the effective range of our proposed system is

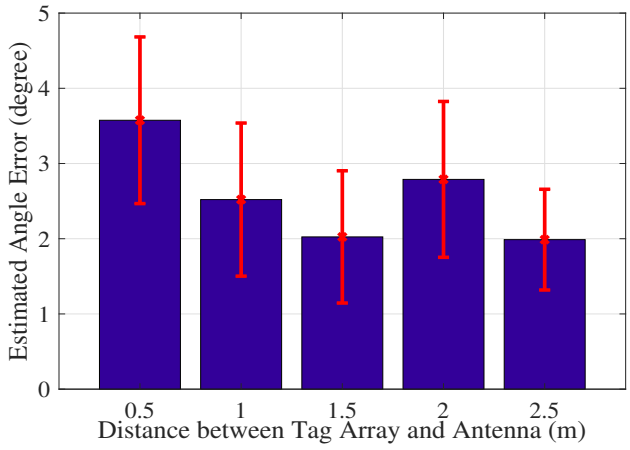

Fig. 22. Impact of the distance between the tag array and the antennas.

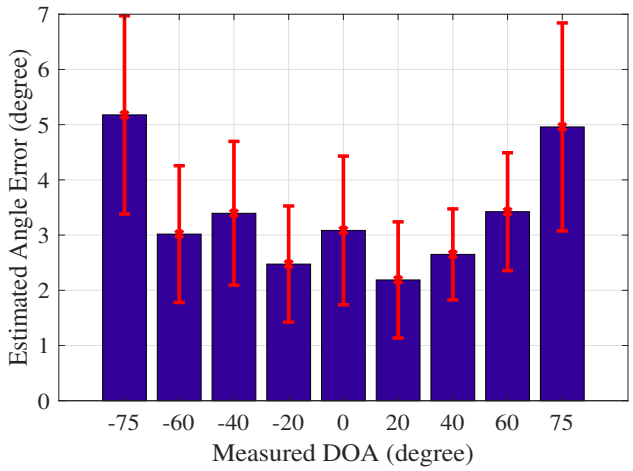

Fig. 23. Impact of different ground truth DOA values.

from 0.5 m to 2.5 m and the effective range of estimated DOA should be between -75° and 75°.

5 Related Work

With the rapid development of Internet of Things, indoor localization attracts increasing attention in recent years. As an RFID-based indoor localization system, our work is closely related to the RF based localization techniques in prior work. In this section we mainly focus on WiFi based techniques and RFID based techniques.

WiFi signals are widely utilized for indoor localization because of its low-cost, wide coverage, and ubiquitous deployment. Among various techniques, Angle of Arrival (AoA) is a typical method to estimate the location of the transmitter [28], but the accurate AoA is hard to estimate because of the multipath effect on the WiFi signal. To mitigate the multipath effect, antenna array-based systems are proposed to estimate the angle of multiple incoming paths of WiFi signal and distinguish the Line-of-sight (LoS) component [23], [29]. In addition, rather than directly calculate the AoA of the LOS path, some prior works leverage machine learning to estimate the position of the transmitter by learning the location features from collected channel state data. For example, Radar is is a WiFi fingerprinting scheme using RSS [30]. Channel State Information (CSI) is regarded as fine-grained representation of the WiFi channel and can achieve more accurate localization performance [31], [32]. However, a well-trained neural network is usually sensitive to changes in the environment, the network parameters need to be updated once the testing environment is changed. Compared with these antenna array based systems, our sparse tag array can achieve high resolution of angle estimation as well as having a low cost.

TABLE 2
Features in Different RFID Tag Localization Techniques

Localization Technique	Hardware Modification	Tag Array	Antenna Array	Dynamic Tags or Antennas
LANDMARC	No	No	Yes	No
RF-IDraw	No	No	Yes	No
Tagoram	No	No	No	Yes
RFfind	Yes	No	No	No
SparseTag	No	Yes	No	No

The RFID technology has been regarded as an effective and low-cost solution for many emerging IoT applications [33]–[38]. Although RFID-based systems are limited by the short communication range, the multipath effect on RFID systems is usually much smaller than that on WiFi systems. Thus, various RFID based localization schemes have been proposed to achieve higher accuracy and convenient deployment than WiFi-based systems.

Existing works on RFID tag localization can be classified into received signal strength Indicator (RSSI)-based and phase-based methods. These works mainly focus on locating a single tag, i.e., one tag is located at a time. For RSSI-based methods, a large number of reference tags are deployed at known locations. By comparing the RSSI data with reference tags, the position of the target tag can be determined [2]. In fact, RSSI values are raw channel information and are not stable, due to the factors such as multipath propagation, tag's orientation, RFID reader's transmit power, etc. RSSI based methods usually do not achieve high accuracy in indoor localization. On the other hand, phase based methods have been developed for estimating distance and direction of arrival (DOA) [3]. However, the measured phase is periodic, which leads to phase ambiguity and makes it less useful. Moreover, considerable measured phase errors are introduced by the reader antennas and the tag itself.

To address these issues, the synthetic aperture radar (SAR) technique is proposed for DOA estimation by moving the reader antenna around [5]. The second solution is the hologram technique, which computes the probability of each known position as the tag source within an area of interest and then chooses the most likely position as the tag location [6], [7]. Another solution is the hyperbolic-based method for distance estimation, which locates a static tag [4]. However, this solution does not achieve high localization accuracy due to limited number of reader antennas. In addition, the RFind system achieves higher localization accuracy using a large virtual bandwidth to estimate time-of-flight, but it requires a special hardware [39]. The features of several state-of-the-art RFID tag localization techniques are summarized in Table 2.

6 Conclusions

In this paper, we investigated the problem of localizing an RFID tag array. The proposed system was termed SparseTag, i.e., a sparse RFID tag array system for high accuracy backscatter indoor localization. The SparseTag system comprised four key components: (i) sparse array processing, (ii) difference co-array design, (iii) DOA estimation using a spatial smoothing method, and (iv) a DOA-based localization method. We implemented the SparseTag system using off-the-shelf RFID tags and reader, and assessed its performance with extensive experiments in two settings. The experimental results validated the effectiveness and high location accuracy of the proposed SparseTag system.

References

[1] C. Yang, X. Wang, and S. Mao, "SparseTag: High-precision backscatter indoor localization with sparse RFID tag arrays," in *Proc. IEEE SECON 2019*, Boston, MA, June 2019, pp. 1–9.

[2] L. M. Ni, Y. Liu, Y. C. Lau, and A. P. Patil, "LANDMARC: Indoor location sensing using active RFID," in *Proc. IEEE PerCom 2003*, Dallas, TX, Mar. 2003, pp. 407–415.

[3] J. Wang, D. Vasisht, and D. Katabi, "RF-IDraw: Virtual touch screen in the air using RF signals," in *ACM SIGCOMM Comput. Commun. Rev.*, vol. 44, no. 4, Oct. 2014, pp. 235–246.

[4] T. Liu, L. Yang, Q. Lin, Y. Guo, and Y. Liu, "Anchor-free backscatter positioning for RFID tags with high accuracy," in *Proc. IEEE INFOCOM 2014*, Toronto, Canada, Apr./May 2014, pp. 379–387.

[5] J. Wang and D. Katabi, "Dude, where's my card? RFID positioning that works with multipath and non-line of sight," in *ACM SIGCOMM Comput. Commun. Rev.*, vol. 43, no. 4, Oct. 2013, pp. 51–62.

[6] L. Yang, Y. Chen, X.-Y. Li, C. Xiao, M. Li, and Y. Liu, "Tagoram: Real-time tracking of mobile RFID tags to high precision using COTS devices," in *Proc. ACM MobiCom 2014*, Maui, HI, Sept. 2014, pp. 237–248.

[7] L. Shangguan and K. Jamieson, "The design and implementation of a mobile RFID tag sorting robot," in *Proc. ACM MobiSys 2016*, Singapore, June 2016, pp. 31–42.

[8] Y. Zhang, M. G. Amin, and S. Kaushik, "Localization and tracking of passive RFID tags based on direction estimation," *Hindawi Int. J. Antennas Propagation*, vol. 2007, p. Article ID 017426, Dec. 2007.

[9] T. Wei and X. Zhang, "Gyro in the air: tracking 3d orientation of batteryless internet-of-things," in *Proc. ACM MobiCom 2016*, New York, NY, Oct. 2016, pp. 55–68.

[10] H. Jin, Z. Yang, S. Kumar, and J. I. Hong, "Towards wearable everyday body-frame tracking using passive RFIDs," *Proc. ACM on Interactive, Mobile, Wearable and Ubiquitous Technol.*, vol. 1, no. 4, p. No. 145, Dec. 2018.

[11] Y. Zhang, L. Xie, Y. Bu, Y. Wang, J. Wu, and S. Lu, "3-Dimensional localization via RFID tag array," in *Proc. IEEE MASS 2017*, Orlando, FL, Oct. 2017, pp. 353–361.

[12] Y. Bu, L. Xie, J. Liu, B. He, Y. Gong, and S. Lu, "3-Dimensional reconstruction on tagged packages via RFID systems," in *Proc. IEEE SECON 2017*, San Diego, CA, June 2017, pp. 1–9.

[13] F. Guidi, N. Decarli, S. Bartoletti, A. Conti, and D. Dardari, "Detection of multiple tags based on impulsive backscattered signals," *IEEE Trans. Commun.*, vol. 62, no. 11, pp. 3918–3930, 2014.

[14] M. Bolic, M. Rostamian, and P. M. Djuric, "Proximity detection with RFID: A step toward the internet of things," *IEEE Pervasive Computing*, vol. 14, no. 2, pp. 70–76, Apr. 2015.

[15] H. Ding, J. Han, C. Qian, F. Xiao, G. Wang, N. Yang, W. Xi, and J. Xiao, "Trio: Utilizing tag interference for refined localization of passive RFID," in *Proc. IEEE INFOCOM 2018*, Honolulu, HI, Apr. 2018, pp.828–836.

[16] F. Xiao, Z. Wang, N. Ye, R. Wang, and X.-Y. Li, "One more tag enables fine-grained RFID localization and tracking," *IEEE/ACM Trans. Netw.*, vol. 26, no. 1, pp. 161–174, Jan. 2018.

[17] R. Schmidt, "Multiple emitter location and signal parameter estimation," *IEEE Trans. Antennas Propag.*, vol. 34, no. 3, pp. 276–280, Mar. 1986.

[18] Impinj Support Portal, "Low level user data support," 2013, Impinj Speedway Revolution Reader Application, [online] Available: https://support.impinj.com.

[19] D. M. Dobkin, *The RF in RFID: UHF RFID in Practice*. London, UK: Newnes, 2012.

[20] F. Lu, X. Chen, and T. Y. Terry, "Performance analysis of stacked RFID tags," in *Proc. 2009 IEEE Int. Conf. RFID*, Orlando, FL, Apr. 2009, pp. 330–337.

[21] S. Pradhan, E. Chai, K. Sundaresan, L. Qiu, M. A. Khojastepour, and S. Rangarajan, "Rio: A pervasive RFID-based touch gesture interface," in *Proc. ACM MobiCom 2017*, Snowbird, UT, Oct. 2017, pp. 261–274.

[22] Y. Tanaka, Y. Umeda, O. Takyu, M. Nakayama, and K. Kodama, "Change of read range for uhf passive rfid tags in close proximity," in *Proc. 2009 IEEE Int. Conf. RFID*, Orlando, FL, Apr. 2009, pp. 338–345.

[23] J. Xiong and K. Jamieson, "Arraytrack: A fine-grained indoor location system," in *Proc. USENIX NSDI 2013*, Lombard, IL, Apr. 2013, pp. 71–84.

[24] P. Pal and P. Vaidyanathan, "Nested arrays: A novel approach to array processing with enhanced degrees of freedom," *IEEE Trans. Signal Process.*, vol. 58, no. 8, pp. 4167–4181, Aug. 2010.

[25] A. Moffet, "Minimum-redundancy linear arrays," *IEEE Trans. Antennas Propag.*, vol. 16, no. 2, pp. 172–175, Mar. 1968.

[26] P. P. Vaidyanathan and P. Pal, "Sparse sensing with co-prime samplers and arrays," *IEEE Trans. Signal Process.*, vol. 59, no. 2, pp. 573–586, Feb. 2011.

[27] C.-L. Liu and P. Vaidyanathan, "Super nested arrays: Linear sparse arrays with reduced mutual coupling–Part I: Fundamentals," *IEEE Trans. Signal Process.*, vol. 64, no. 15, pp. 3997–4012, Aug. 2016.

[28] S. Sen, J. Lee, K.-H. Kim, and P. Congdon, "Avoiding multipath to revive inbuilding WiFi localization," in *Proc. ACM MobiSys 2013*, Taipei, Taiwan, June 2013, pp. 249–262.

[29] W. Gong and J. Liu, "Robust indoor wireless localization using sparse recovery," in *Proc. IEEE ICDCS 2017*, Atlanta, GA, June 2017, pp. 847–856.

[30] P. Bahl and V. Padmanabhan, "Radar: An in-building rf-based user location and tracking system," in *Proc. IEEE INFOCOM 2000*, Tel Aviv, Israel, Apr. 2000, pp. 775–784.

[31] X. Wang, L. Gao, and S. Mao, "CSI phase fingerprinting for indoor localization with a deep learning approach," *IEEE Internet of Things Journal*, vol. 3, no. 6, pp. 1113–1123, Dec. 2016.

[32] X. Wang, X. Wang, and S. Mao, "Indoor fingerprinting with bimodal CSI tensors: A deep residual sharing learning approach," *IEEE Internet of Things J.*, vol. 8, no. 6, pp. 4498–4513, Mar. 2021.

[33] C. Yang, X. Wang, and S. Mao, "Unsupervised detection of apnea using commodity RFID tags with a recurrent variational autoencoder," *IEEE Access J.*, vol. 7, no. 1, pp. 67 526–67 538, June 2019.

[34] X. Wang, J. Zhang, Z. Yu, S. Mao, S. Periaswamy, and J. Patton, "On remote temperature sensing using commercial UHF RFID tags," *IEEE Internet of Things J.*, vol. 6, no. 6, pp. 10 715–10 727, Dec. 2019.

[35] J. Zhang, Z. Yu, X. Wang, Y. Lyu, S. Mao, S. Periaswamy, J. Patton, and X. Wang, "RFHUI: An RFID based human-unmanned aerial vehicle interaction system in an indoor environment," *KeAi Digital Commun. Netw. J.*, vol. 6, no. 1, pp. 14–22, Feb. 2020.

[36] C. Yang, X. Wang, and S. Mao, "RFID-Pose: Vision-aided 3D human pose estimation with RFID," *IEEE Transactions on Reliability*, vol. 70, no. 3, pp. 1218–1231, Sept. 2021.

[37] C. Yang, X. Wang, and S. Mao, "RFID based 3D human pose tracking: A subject generalization approach," *Elsevier/KeAi Digital Communications and Networks*, in press. DOI: 10.1016/j.dcan.2021.09.002.

[38] C. Yang, L. Wang, X. Wang, and S. Mao, "Environment adaptive RFID based 3D human pose tracking with a meta-learning approach," revised for journal publication.

[39] Y. Ma, N. Selby, and F. Adib, "Minding the billions: Ultra-wideband localization for deployed rfid tags," in *Proc. ACM MobiCom 2017*, Snowbird, UT, Oct. 2017, pp. 248–260.